Human Molecular Genetics, 2020, Vol. 29, No. 2 177–188

doi: 10.1093/hmg/ddz211
Advance Access Publication Date: 7 September 2019
General Article

GENERAL ARTICLE

Impaired turnover of hyperfused mitochondria in severe axonal neuropathy due to a novel DRP1 mutation

Fabiana Longo[1,†], Sara Benedetti[2,†], Alberto A. Zambon[3], Maria Grazia Natali Sora[3], Chiara Di Resta[4,5], Daniele De Ritis[1], Angelo Quattrini[3,6], Francesca Maltecca[1,4,*], Maurizio Ferrari[2,4,5,‡] and Stefano Carlo Previtali[3,6,‡]

[1]Neurogenomics Unit, Division of Neuroscience, IRCCS Ospedale San Raffaele, Milan, Italy, [2]Laboratory of Clinical Molecular Biology and Cytogenetics, IRCCS Ospedale San Raffaele, Milan, Italy, [3]Department of Neurology, IRCCS Ospedale San Raffaele, Milan, Italy, [4]Università Vita-Salute San Raffaele, Milan, Italy, [5]Genomic Unit for the Diagnosis of Human Pathologies, Division of Genetics and Cellular Biology IRCCS Ospedale San Raffaele, Milan, Italy and [6]Inspe and Division of Neuroscience, IRCCS Ospedale San Raffaele, Milan, Italy

*To whom correspondence should be addressed at: Tel: +39 0226439116; +39 0226434777; Fax: +39 0226436352; Email: maltecca.francesca@hsr.it.

Abstract

Mitochondria undergo continuous cycles of fusion and fission in response to physiopathological stimuli. The key player in mitochondrial fission is dynamin-related protein 1 (DRP1), a cytosolic protein encoded by *dynamin 1-like* (*DNM1L*) gene, which relocalizes to the outer mitochondrial membrane, where it assembles, oligomerizes and drives mitochondrial division upon guanosine-5′-triphosphate (GTP) hydrolysis. Few DRP1 mutations have been described so far, with patients showing complex and variable phenotype ranging from early death to encephalopathy and/or optic atrophy. The disease is the consequence of defective mitochondrial fission due to faulty DRP1 function. However, the underlying molecular mechanisms and the functional consequences at mitochondrial and cellular level remain elusive. Here we report on a 5-year-old girl presenting psychomotor developmental delay, global hypotonia and severe ataxia due to axonal sensory neuropathy harboring a novel *de novo* heterozygous missense mutation in the GTPase domain of DRP1 (NM_012062.3:c.436G>A, NP_036192.2: p.D146N variant in *DNM1L*). Patient's fibroblasts show hyperfused/balloon-like giant mitochondria, highlighting the importance of D146 residue for DRP1 function. This dramatic mitochondrial rearrangement phenocopies what observed overexpressing DRP1-K38A, a well-known experimental dominant negative version of DRP1. In addition, we demonstrated that p.D146N mutation has great impact on peroxisomal shape and function. The p.D146N mutation compromises the GTPase activity without perturbing DRP1 recruitment or assembly, causing decreased mitochondrial and peroxisomal turnover. In conclusion, our findings highlight the importance of sensory neuropathy in the clinical spectrum of *DRP1* variants and, for the first time, the impact of *DRP1* mutations on mitochondrial turnover and peroxisomal functionality.

[†]F.L. and S.B. share first coauthorship
[‡]M.F. and S.C.P. share last coauthorship

Received: March 26, 2019. **Revised:** August 9, 2019. **Accepted:** August 28, 2019

Introduction

Mitostasis is a specialized form of cellular homeostasis that maintains mitochondrial number, shape and quality. It is ensured by mitochondrial dynamics, a balance between fission and fusion events able to keep mitochondria in a regulated shape and network (1,2). Mitochondrial dynamics determines mitochondrial turnover, as proper mitochondrial fission is a prerequisite for engulfment by autophagosomes during mitophagy (3). Mitostasis is crucial in neurons, since they need to preserve mitochondrial pool throughout their entire life and to supply healthy mitochondria to neuronal distal processes (2). Therefore, mutations in proteins involved in mitostasis cause neurodegenerative disorders, highlighting a specific neuronal susceptibility to mitochondrial impairment (2).

Main players of mitochondrial dynamics are dynamin superfamily proteins, and among these, dynamin-related protein 1 (DRP1) is the driver of mitochondrial fission. DRP1 is a cytosolic protein that relocalizes to the outer mitochondrial membrane (OMM), oligomerizing and driving mitochondrial constriction upon guanosine-5′-triphosphate (GTP) hydrolysis (1). Main functional DRP1 units are a GTPase domain providing the mechanical force for membrane constriction and a middle domain mediating DRP1 oligomerization (1). DRP1 also mediates peroxisomal fission, which is critical for maintaining peroxisome shape and function (4). A strong interplay between mitochondria and peroxisomes exists, in terms of regulation of abundance, metabolic pathways and compensatory responses in disease (4,5).

Mutations in DRP1 result in severe and complex neurological disorders still lacking a complete comprehension of the pathogenetic mechanism. *De novo* heterozygous mutations in the middle domain cause progressive encephalopathy with developmental delay and epilepsy as result of a possible dominant negative mechanism affecting protein oligomerization and/or OMM recruitment (6–14). Biallelic mutations in the GTPase domain usually cause lethal infantile encephalopathy due to loss of function mechanism still preventing DRP1 oligomer formation (15–18), whereas heterozygous mutations associate with milder phenotype restricted to optic atrophy (19). Only recently, the p.G32A heterozygous mutation in the GTPase domain has been reported in a 7-year-old child with developmental delay, hypotonia, sensory neuropathy and optic atrophy due to a dominant negative effect probably acting on DRP1 mitochondrial recruitment (20).

Here we describe a *de novo* heterozygous missense mutation in the GTPase domain of DRP1, the p.D146N, affecting a 5-year-old girl presenting a severe psychomotor developmental delay, global hypotonia and severe ataxia due to axonal sensory neuropathy. Our findings show that p.D146N DRP1 properly oligomerizes but prevents GTPase function, causing dramatic mitochondrial and peroxisomal elongation. The enormous mitochondrial spheres caused by p.D146N mutation undergo aberrant turnover despite functional autophagic flux and accumulate oxidative stress.

Collectively, our results expand the spectrum of neurological syndromes caused by DRP1 mutations and highlight the importance of D146 residue for DRP1 functionality on mitochondrial and cellular physiology.

Results

Case report

The proband is a Caucasian girl born to non-consanguineous parents by cesarean section at 43 gestational weeks. Pregnancy was characterized by threatened abortion and pyelonephritis of the mother. Family history was mute for neuromuscular and metabolic disorders. Apgar score was 8 and 9 at 1 and 5 minutes after birth, respectively. Postnatal period was regular. Since the first weeks of life, she failed to attain developmental milestones. Neither head nor trunk control was acquired by the first year of life.

She was admitted to a local hospital for the first time at the age of 16 months. Neurological examination revealed severe global developmental delay. Head control was incomplete. Head circumference was normal for age. Neither rolling nor sitting was possible. Polysyllabic consonant babbling was present, but no spontaneous words were recorded. Severe global hypotonia with mild distal spasticity of the limbs was observed (Fig. 1A and B). Deep tendon reflexes were markedly reduced. Myoclonic spasms of the left hand were noticed, although electrical abnormalities were excluded by video electroencephalography. Brain magnetic resonance imaging (MRI) was normal. Routine blood tests, urine analysis, ophthalmologic examination and abdomen and cardiac ultrasound were normal. Serum lactate was slightly elevated (2.44 mmol/L; control range, 0.7–2.1 mmol/L). Laboratory tests to rule out hereditary amino acidopathies, organic acidurias and defects of mitochondrial beta-acidification resulted normal. Nerve conduction study and needle examination of the muscle were inconclusive. Genetic analyses to exclude spinal muscular atrophy and Prader-Willi syndrome were negative.

Four months later, she was referred to our center. We performed a muscle biopsy that excluded an underlying myopathy showing only mild lipid storage (Fig. 1C–G). Electroneuronography was repeated and revealed severe axonal sensory neuropathy; motor conduction parameters and compound motor action potentials were normal. Normal brain MRI was confirmed at 30 months of age.

On last examination (at age 5 years), the child was alert, pleasant and collaborative and was able to create two-word sentences with mildly slurred speech. Weight was under the fifth percentile (12 kg). Cranial nerves were normal except for mildly saccadic smooth pursuit eye movements and lower facial weakness. Occasional coughing while drinking liquids was reported, but no dysphagia for solids was recorded. Head control was only partially achieved. Global hypotonia and lack of trunk control were observed. No signs of scoliosis or contractures were present. All four limbs displayed ligamentous laxity, reduced muscle bulk, reduced tone with a slight 'catch' of lower limbs' extensors distally (Fig. 1A and B). Spontaneous movements were poor, but she was able to lift her arms against gravity and bring a spoon to her mouth autonomously. Segmental muscle strength was hardly evaluable due to scarce compliance and language barrier. Severe sensory ataxia of upper and lower limbs was present causing pseudo athetoid movements. Deep tendon reflexes were not evocable. Plantar responses were mute. Thermal and pain sensitivity was preserved, and no skin ulcers were detected.

Clinical exome sequencing and identification of DRP1 mutation

Proband and parent samples were enriched with TruSight One clinical exome panel and analyzed using Illumina MiSeq. Mean cluster density was 1359 k/mm^2. After paired-end sequencing, we obtained an average of 175 million reads and >96% of the entire target covered by at least 20 reads. Mean coverage depth was 120×.

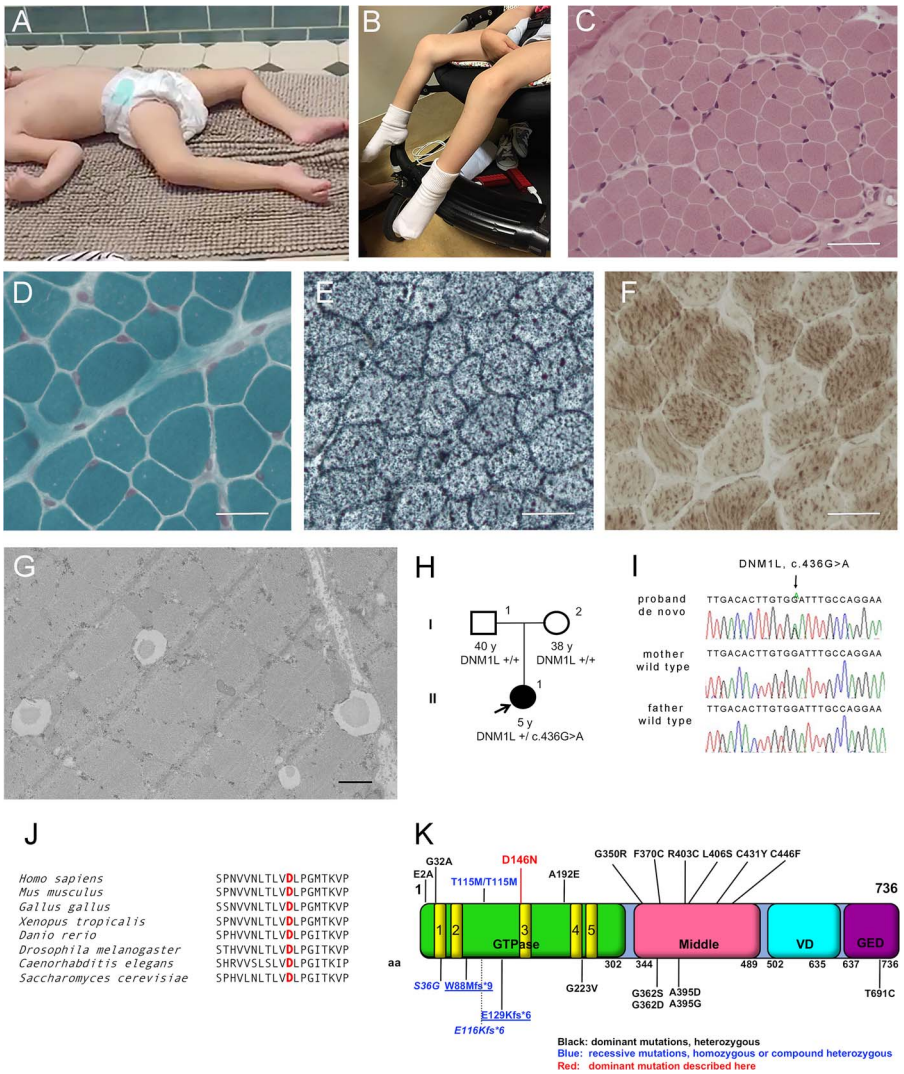

Figure 1. p.D146N patient mutation and features. (**A**) Images of p.D146N patient showing diffuse hypotonia at 2 years old and (**B**) at 5 years old. Muscle biopsy images of p.D146N patient including hematoxylin and eosin (**C**) and Gomori trichrome (**D**) showing normal fiber variability and normal nuclei disposition; Sudan black showing mild lipid storage into the muscle fibers (**E**); combined cytochrome oxidase/succinic dehydrogenase showing normal enzymatic activity (**F**). (**G**) Electron microscopy showing normal sarcomere distribution. (**H**) Family pedigree of p.D146N patient family indicates *de novo* heterozygous mutation. The arrow indicates the proband. Blackened symbols denoted affected member, and unblackened symbols denote unaffected individuals. Circles and squares indicate females and males, respectively. (**I**) Sanger sequencing confirmation of the presence of the *DNM1L* variant in the proband (heterozygous) compared with wild-type sequence in the parents. (**J**) D146 DRP1 residue conservation among different DRP1 orthologs. (**K**) DRP1 gene scheme with functional domains, reporting the mutations described so far (6–20,44,45). Conserved GTP binding motifs, shared for all dynamin members, are shown in the GTPase domain in yellow and are indicated by numbers. aa: amino acid.

Overall, over 14 000 variants, including small insertions–deletions and single nucleotide variations, were identified for each family member. Variants were filtered as detailed in Materials and Methods. Trio analysis allowed to prioritize variants according to different inheritance models and relevance to the clinical phenotype. We identified the NM_012062.3:c.436G>A missense variant in the *dynamin 1-like* [*DNM1L*)/*DRP1* gene Online Mendelian Inheritance in Man (OMIM)* 603850], causing the amino acidic substitution NP_036192.2: p.D146N (Fig. 1H and I). This variant was classified as class IV (likely pathogenic) according to the American College of Medical Genetics and Genomics (ACMG) criteria: it had not been previously identified in control populations [ExAC, 1000G, double-strand Single nucleotide polymorphisms (dbSNP)]; it involved a highly conserved nucleotide according to phyloP (residue conservation among different species reported in Fig. 1J); it localized in a functional GTPase protein domain [Fig. 1K and (21)]; it was predicted as deleterious by different *in silico* prediction software; it was present only in the affected child and not in the parents (*de novo*; Fig. 1H and I).

p.D146N mutation causes dramatic mitochondrial network hyperfusion acting through a dominant negative mechanism

We investigated the molecular consequences of p.D146N mutation at DRP1 protein level. We derived human primary fibroblasts from p.D146N patient skin biopsy and used neonatal skin-derived primary fibroblasts as controls. By performing western blot (WB) experiments, we found no difference in the amount of DRP1 protein in the monomeric form in p.D146N patient as compared to controls (Fig. 2A). Since DRP1 activity depends on its oligomerization, we also analyzed the high-order complexes of DRP1 [those actively mediating mitochondrial

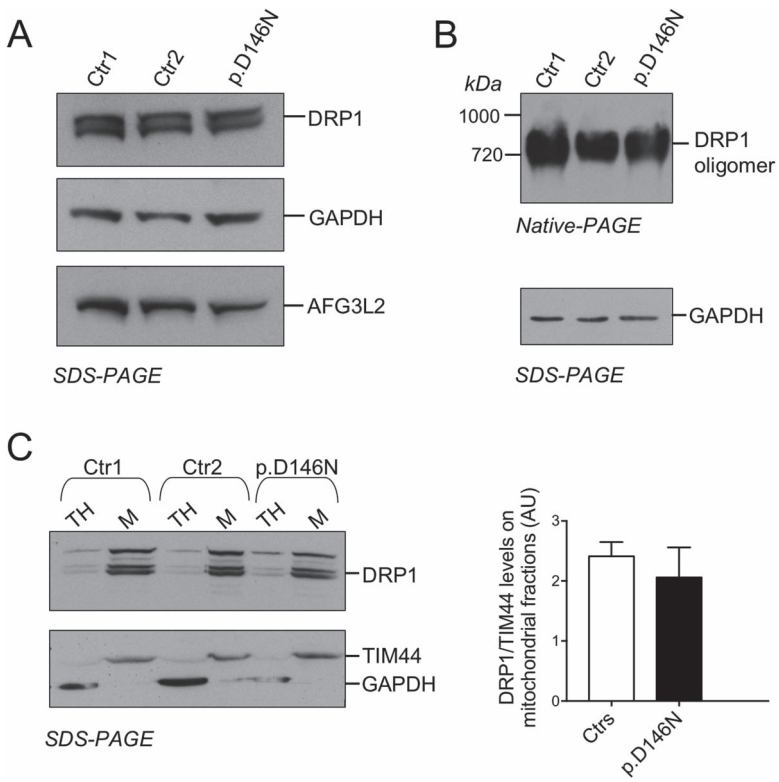

Figure 2. p.D146N DRP1 protein is stable, oligomerizes and is recruited on mitochondrial outer membrane. (**A**) DRP1 monomer analysis in SDS-PAGE followed by WB, comparing the patient with two age-matched healthy fibroblasts as controls, normalized on GAPDH (cytosolic marker) and AFG3L2 (mitochondrial marker). (**B**) DRP1 oligomer analysis in Native-PAGE followed by WB, normalized on GAPDH in SDS-PAGE. (**C**) Representative experiment showing DRP1 recruitment on mitochondrial fraction in the patient and controls. Mitochondrial fractions were purified and checked by TIM44 as mitochondrial marker and GAPDH as cytosolic marker. Graph on the right shows the quantification of three independent experiments. Ctr: control, TH: total homogenate, Mito: mitochondrial fraction, AU: arbitrary units.

fission (1)] in Native–polyacrylamide gel electrophoresis (PAGE), and we found no difference in p.D146N patient compared to controls (Fig. 2B). In order to study if DRP1 recruitment on mitochondria could be affected in p.D146N, we purified mitochondrial fractions from p.D146N patient and control fibroblasts, and we revealed no alteration in the amount of DRP1 recruited on mitochondria (Fig. 2C).

We then analyzed how p.D146N mutation impacts mitochondrial network morphology. By infecting cells with mito-DsRed2, we labeled mitochondrial network and then performed live imaging analysis. We found mitochondria in p.D146N patient to be enormously hyperfused, leading to the formation of giant balloon-like organelles, never seen in control cells (Fig. 3A). Altogether, these results suggest that the effect of p.D146N DRP1 is comparable to a dominant negative, totally masking the wild-type allele function. To confirm this hypothesis, we transfected control cells with pEYFP (enhanced yellow fluorescent protein)–Mito construct plus the artificial dominant negative DRP1 construct (DRP1-K38A, (22)) and compared the resulting mitochondrial network with the one observed in p.D146N patient fibroblasts. Strikingly, we found a comparable phenotype, since DRP1-K38A presented giant hyperfused and balloon-shaped mitochondria as those seen in p.D146N fibroblasts (Fig. 3B).

We also overexpressed p.D146N DRP1 in wild-type fibroblasts, and we observed the same striking signs of mitochondrial hyperfusion (Fig. 3C) previously detected in p.D146N patient cells (Fig. 3A and B), further enforcing the evidence of a dominant negative mechanism. Overexpression of p.G32A DRP1 [mutation in the GTPase domain (20)] or p.L406S DRP1 [mutation in the middle domain (17)] in wild-type cells led again to mitochondrial hyperfusion, whereas this was not observed by the overexpression of wild-type DRP1 (Fig. 3C and D). Electron microscopy (EM) experiments further confirmed marked mitochondrial hyperfusion in p.D146N patient fibroblasts (Fig. 3E, arrows).

Overall these results suggest a common dominant negative–pathogenetic mechanism for these mutations.

p.D146N shows reduced mitochondrial turnover despite normal autophagic flux, with increased mitochondrial reactive oxygen species

Efficient mitochondrial fission is a necessary event for mitochondrial turnover and degradation (31). To analyze mitochondrial turnover in p.D146N fibroblasts, we used the Tet-ON inducible version of MitoTimer construct (pTRE-Tight-MitoTimer). By doxycycline pulse, Tet-ON MitoTimer allows to synchronize its expression into mitochondria. In physiological conditions, MitoTimer maturation over time results in a fluorescence shift from green to red, indicative of protein maturation. The disappearance of the red fluorescence of mature MitoTimer can be correlated to mitochondrial degradation by mitophagy ((23) and Fig. 4A). By live imaging, we acquired three different time points of MitoTimer fluorescence in transfected cells (4 hours to follow its first expression (data not shown) and 28 and 52 hours from doxycycline pulse to count the loss of the red fluorescence signal). Interestingly, we found that p.D146N cells have a marked slowing of mitochondrial turnover compared to controls, presenting a lower percentage of cells lacking the red fluorescence over time (Fig. 4B). These data

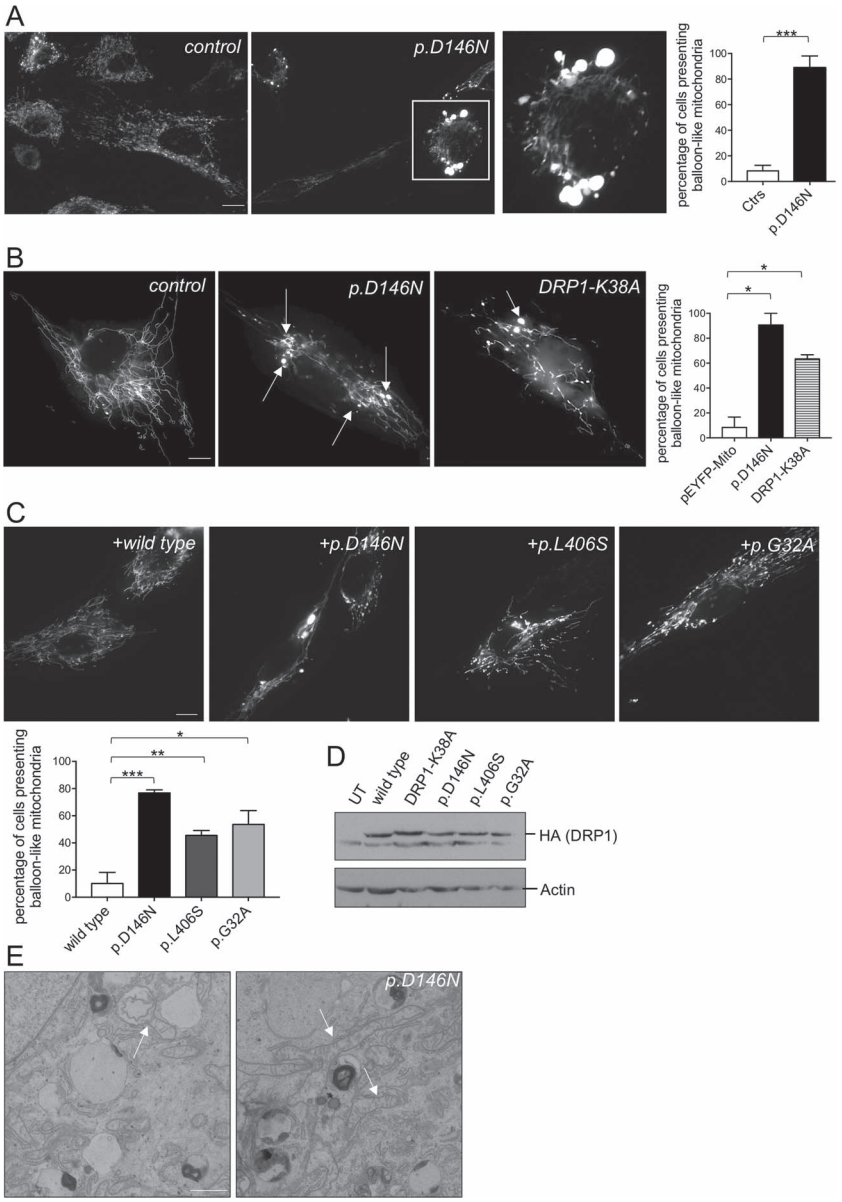

Figure 3. p.D146N DRP1 mutation leads to dramatic mitochondrial hyperfusion in patient fibroblasts. (**A**) Representative images of mitochondrial morphology assessed by mito-DsRed2 infection and live imaging acquisition. Graph on the right shows the quantification of three independent experiments (at least 100 cells per experiment). Bar scale: 100 μm. (**B**) Representative images of mitochondrial morphology, assessed by pEYFP-Mito + empty pcDNA3 or pEYFP-Mito + pcDNA3-DRP1-K38A construct transfection and live imaging acquisition. Graph on the right shows the quantification of three independent experiments). (**C**) Live imaging images of wild-type fibroblasts overexpressing wild-type DRP1 (as control) and different mutant DRP1 constructs (p.D146N, p.G32A and p.L406S), all cotransfected with pEYFP-Mito Vector to visualize mitochondria in a ratio of 2:1. Quantification graph on the bottom three independent experiments. Mean ± SEM; $^{*}P < 0.05$, $^{**}P < 0.005$, $^{***}P < 0.001$. (**D**) WB showing levels of overexpressed DRP1 (HA tagged) protein relative to **C** (plus DRP1-K38A overexpression, live imaging results not shown). (**E**) Representative images of EM experiments on p.D146N fibroblasts, showing mitochondrial elongation (arrows). Bar scale: 1 μm. UT: untransfected.

indicate that probably the steric hindrance of hyperelongated mitochondria could affect mitophagy. We hypothesized that impaired mitochondrial turnover could result in an attempt of the cell to upregulate degradative systems in order to remove putative damaged mitochondria. We thus studied autophagic flux in p.D146N cells. At steady-state levels, we did not detect any difference in microtubule-associated proteins 1A/1B light chain 3 (LC3)-II levels between patient and control cells. We also evaluated the difference in the amount of LC3-II in the presence and absence of saturating levels of chloroquine (24). This difference is unchanged in the patient versus controls, indicating an equally efficient autophagic flux (Fig. 4C).

Aberrant mitochondrial turnover is known to result in increased oxidative stress in the cell caused by enhanced mitochondrial reactive oxygen species (ROS accumulation (3). We purified mitochondrial fractions and analyzed the levels of oxidized proteins in patient and control cells, by the detection of carbonyl groups introduced into proteins by oxidative reactions. We found that p.D146N cells present a higher level of carbonylated proteins in mitochondrial fractions compared to controls (Fig. 5A).

To determine whether p.D146N DRP1 affects mitochondrial respiration, we measured production in freshly isolated mitochondria at basal level and upon stimulation with pyruvate/-

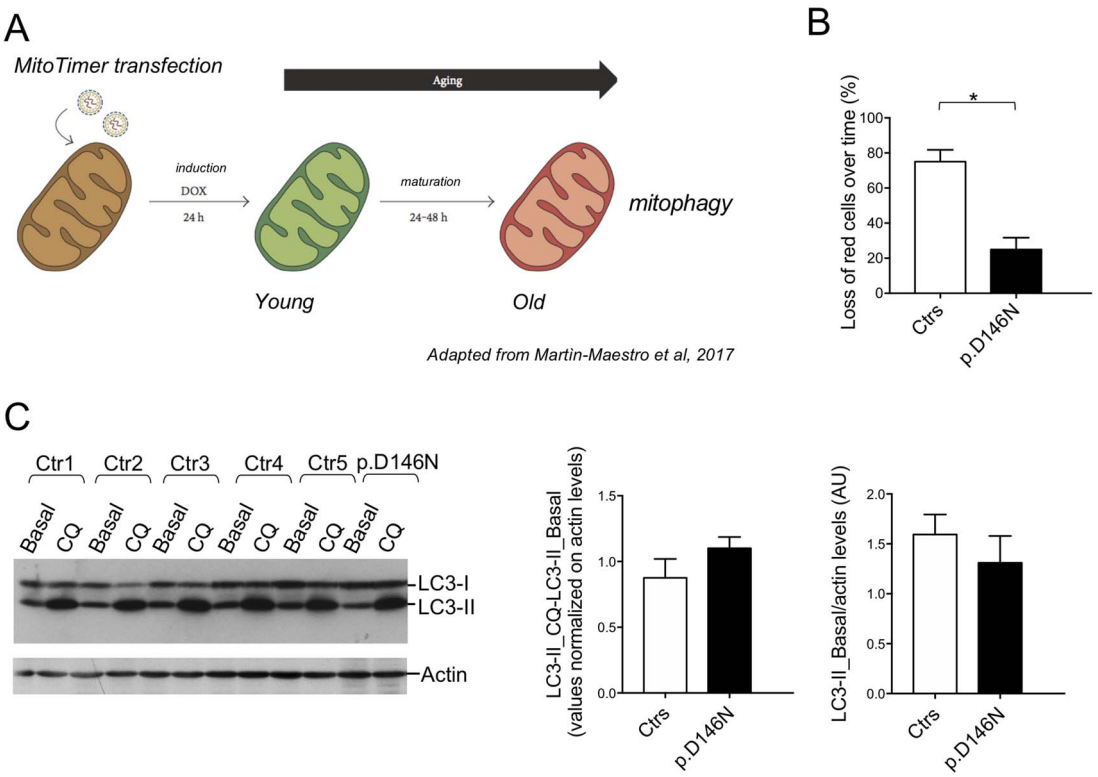

Figure 4. Mitochondrial turnover in p.D146N fibroblasts is reduced. (**A**) Cartoon showing the functioning of the MitoTimer tool. The loss of the red mitochondria-containing cells is due to mitophagic degradation of the organelles. (**B**) Quantification of MitoTimer experiments (expressing pTRE-Tight-MitoTimer construct in fibroblast cells, as described in Materials and Methods) showing the loss of the red fluorescent cells (percentage) of controls and patient. (**C**) WB analysis of autophagic flux (LC3-II turnover normalized on actin levels). Graphs show the difference in LC3-II in the presence or absence of chloroquine (50 μM for 6 hours), values previously normalized on actin and the quantification of LC3-II on actin levels in basal condition, both in the patient and controls (mean ± SEM). DOX: doxycycline, CQ: chloroquine.

malate or glutamate/malate in controls and p.D146N fibroblasts. The mitochondrial ATP levels resulted comparable in these cells in both experimental conditions (Fig. 5B).

p.D146N mutation causes elongation of peroxisomes and increased peroxisomal mass

Being DRP1 function shared by mitochondria and peroxisomes for their division (4), we analyzed peroxisomal network in p.D146N fibroblasts. By immunofluorescence of peroxisomal membrane protein 70 (PMP70), a peroxisomal membrane marker, and confocal microscopy, we noticed a significant elongation of peroxisomes in p.D146N cells, in contrast with the dot-like structures observed in controls (Fig. 6A). We quantified the number of cells presenting elongated peroxisomes, and we found them significantly increased in the presence of p.D146N mutation (Fig 6A). We also assayed by WB the levels of PMP70, and we found them increased, indicating that peroxisomal elongation in p.D146N patient fibroblasts influences peroxisomal turnover (Fig. 6B). Of note, we also detected a striking increase in peroxisomal catalase by WB, the common detoxifying enzyme of peroxisomes (Fig. 6B).

Discussion

We describe a new *de novo* missense mutation (p.D146N) in the GTPase domain of DRP1, affecting a child with hypotonia, psychomotor developmental delay, and severe limb ataxia due to sensory axonal neuropathy. Previous reports describe early lethal encephalopathy in biallelic loss of function mutations in the GTPase domain (15, 16, 18) and rarely in dominant mutations of the middle domain (6, 17). Most of the heterozygous mutations in the DRP1 middle domain cause severe encephalopathy with epilepsy and failure to thrive, reporting a variable range of other aspects including cerebellar ataxia, athetoid movements and dystonia. Conversely, heterozygous mutations in the GTPase domain result only in optic atrophy (19), except for a child recently described (p.G32A mutation) also showing encephalopathy, psychomotor developmental delay, peripheral neuropathy and ulcers (20). From a genetic point of view, our patient constitutes the second description of a heterozygous mutation in the GTPase domain of DRP1 resulting in a complex neurological disorder, including a sensory neuropathy, typical of mitochondrial dysfunction. However, the outcomes of p.D146N mutation at the organellar level are much more severe compared to p.G32A, as discussed later.

As previously reported in other DRP1 mutations (10, 11), we did not observe signs of mitochondrial abnormalities in muscle biopsy neither significant elevation of lactate. Conversely, we observed a progressive neurological impairment involving both the central and peripheral nervous system. Of particular interest is the presence of a severe sensory axonal neuropathy, as documented by nerve conduction studies with the predominant impairment of the proprioceptive sensation (ataxia with pseudoathetosis).

From the clinical point of view, this is the second description of sensory ataxia due to peripheral neuropathy, and interestingly also the other one was due to a heterozygous mutation in the GTPase domain of DRP1. However, neuropathy might be underestimated in other mutated patients, possibly overridden

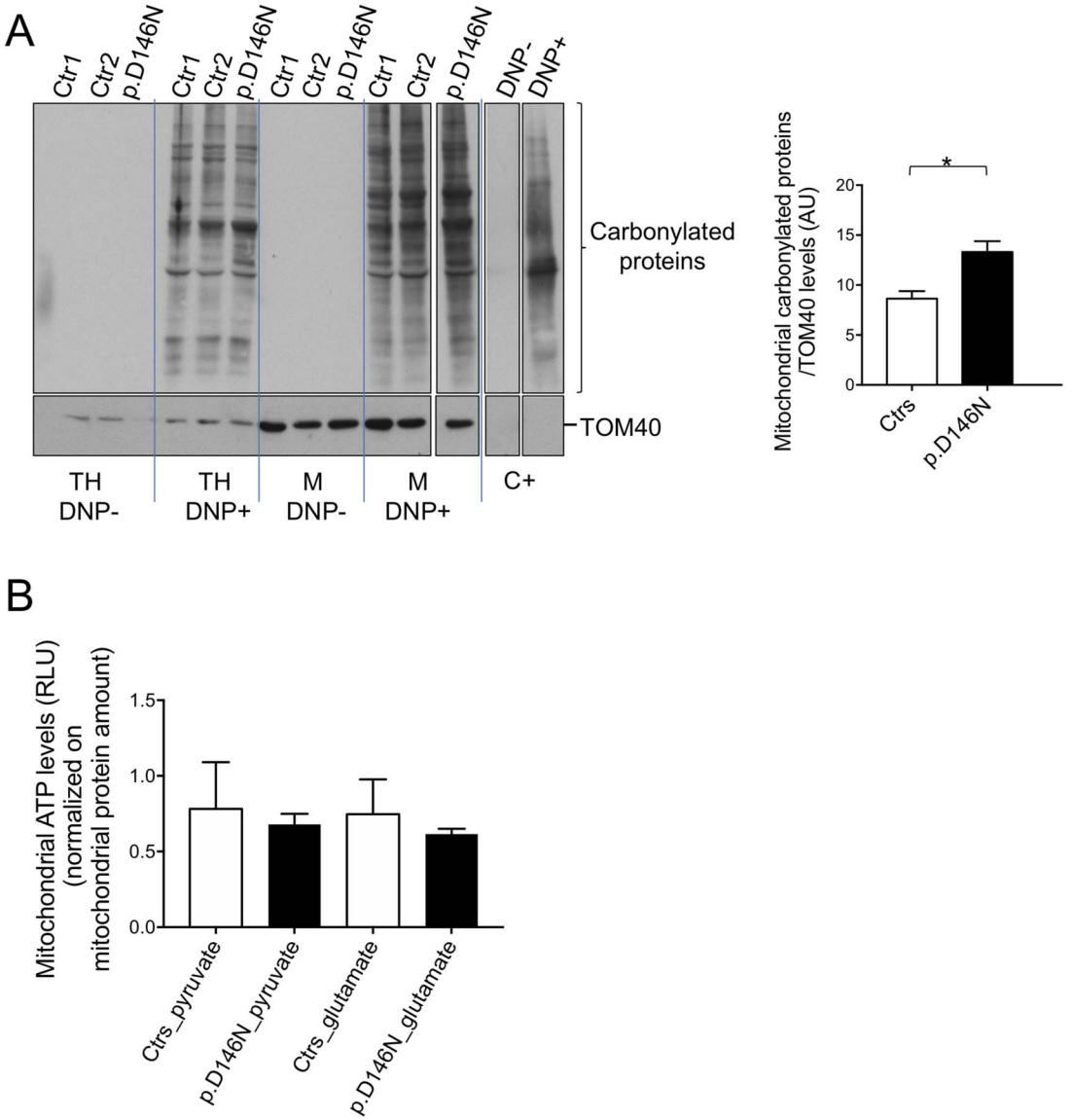

Figure 5. Mitochondrial oxidized proteins are increased, while ATP levels are normal in p.D146N fibroblasts. (**A**) On the left, WB of carbonylated proteins in the patient and controls (both TH and M fractions), normalized on TOM40 levels. DNP+ proteins corresponding to oxidized proteins (carbonylated), were revealed by specific anti-DNP+ antibody. The last two lanes show oxidized proteins from a positive control (C+) prepared by incubating a total homogenate from control fibroblasts with 25 mM N-2-hydroxyethylpiperazine-N′-2-ethanesulfonic acid buffer, pH 7.2; 25 mM ascorbate; 100 μM $FeCl_3$ for 5 hours at 37°C. On the right, the graph shows the quantification of band intensities for DNP+ lanes in mitochondrial fractions of patient and controls in three independent experiments. (**B**) Mitochondrial ATP measurement in the patient and controls, using pyruvate or glutamate as substrates. % Mean ± SEM; $^{*}P < 0.05$.

by severe central nervous system aspects. Accordingly, insensitivity to pain as a possible consequence of a sensory neuropathy was previously described in the p.G362S mutation (11), as well as hypotonia and lack of tendon reflexes in early lethal case (6). Moreover, DRP1 activity was linked to neuropathic pain in animal models (25); sensory neuropathy is well documented in complex mitochondria disorders (26) or represents the primary findings of mitochondria dysfunction such as in POLG1(35) and GDAP1 mutations (27). Finally, recent findings suggest a direct interaction between DRP1 and RAB7 to control mitochondrial dynamics (28), being biallelic mutations of *RAB7* responsible of a predominant sensory Charcot-Marie-Tooth neuropathy (29).

To gain insight into the pathogenetic mechanism of this mutation, we performed a detailed characterization of the outcomes at mitochondrial and peroxisomal level in patient primary fibroblasts. Our results demonstrate that p.D146N mutation dramatically affects mitochondrial and peroxisomal fission leading to extremely hyperfused organelles. These defects affect organellar turnover and cause oxidative stress.

It has been reported that D146 residue has critical function in GTP binding and hydrolysis, as it belongs to a functional GTPase domain consensus motif shared by all dynamin superfamily members (21), highly conserved during evolution. Accordingly, our data show that p.D146N does not affect the amount of DRP1 protein, either as monomer or high order-oligomer, and its recruitment onto OMM. This behavior coherently differs from both DRP1 mutations in the middle domain, which impair DRP1 recruitment on OMM and/or assembly in high-order complexes (7, 10), and from biallelic truncating-DRP1 mutations, in which the protein is presumably not present (15) or reduced (16).

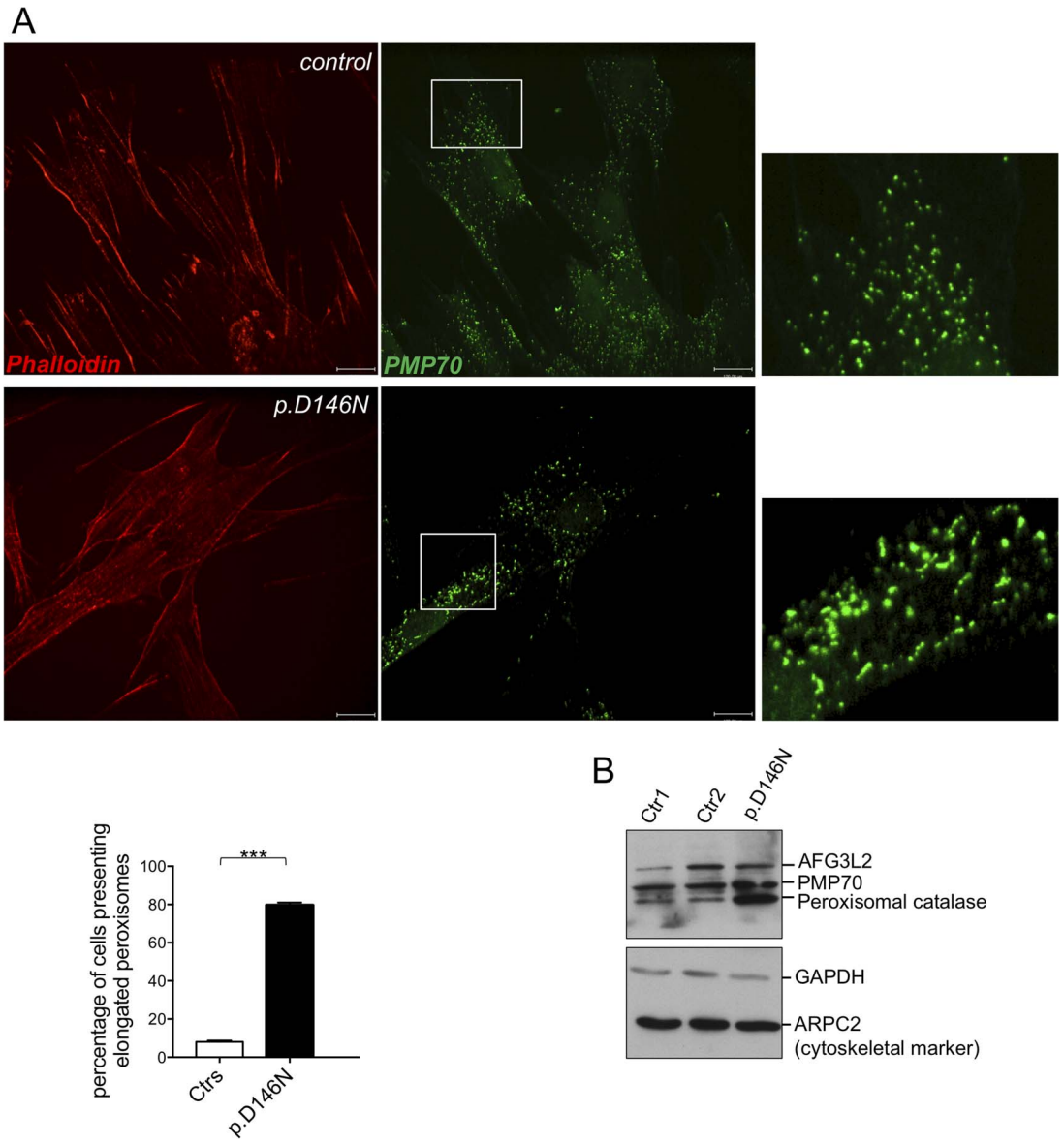

Figure 6. Peroxisomal network rearrangement in p.D146N fibroblasts. (**A**) Representative confocal images of immunofluorescence experiments on patient and controls, labeled with anti-phalloidin to define the cell area (in red) and anti-PMP70 to label peroxisomes (in green). Bar scale: 100 µm. Quantification of cells presenting elongated peroxisomes in patient and control fibroblasts (at least 50 cells per genotype were quantified). Mean ± SEM, $^{***}P < 0.001$. (**B**) WB analysis of peroxisomal mass (PMP70) and peroxisomal catalase, in the patient and controls, normalized on AFG3L2 as mitochondrial marker, GAPDH as cytosolic marker and ARPC2 as cytoskeletal marker.

p.D146N DRP1 is therefore fully competent to mediate the first steps of mitochondrial fission, from assembly to OMM recruitment. However, the dramatic mitochondrial hyperelongation observed in p.D146N patient fibroblasts indicates that p.D146N DRP1 is not able to complete mitochondrial division, likely via blocking the GTP binding activity.

Live imaging analyses on p.D146N patient fibroblasts disclose the presence of giant balloon-like structures, and this extreme phenotype has never been reported so far in patients with DRP1 mutations (6–20). These bulb/balloon-like mitochondria could reflect mitochondrial nucleoid aggregation, as previously reported in condition of DRP1 downregulation (30). Mitochondrial DNA replication is indeed coupled with DRP1-mediated mitochondrial division and is spatially linked to endoplasmic reticulum (ER)–mitochondria contact sites (31).

Our data demonstrate that mitochondrial fission process is totally abolished by DRP1 p.D146N mutation, supporting negative dominance instead of haploinsufficiency as underlying mechanism. Indeed, we found similar giant mitochondria by transfecting the experimentally designed dominant negative version of DRP1 (DRP1-K38A) or p.D146N DRP1 in wild-type fibroblasts. In agreement, functional mapping of DRP1 showed that the D146 is a key residue for stabilizing the conformation of K38 residue, which is involved in phosphate binding, and thus for GTPase activity (21). Finally, *Dnm1l*$^{+/-}$ mouse is viable and fertile and does not present any visible or gross abnormality, while *Dnm1l*$^{-/-}$ mouse is embryonic lethal (32).

Mitochondrial hyperfusion in p.D146N fibroblasts leads to extremely harmful consequences on mitostasis. Indeed,

p.D146N fibroblasts present slowed mitochondrial degradation. This is not the result of an impaired autophagic flux, which we measured unchanged in patient cells versus controls, but is likely due to the steric hindrance of giant mitochondria hampering their complete engulfment by autophagosomes. Interestingly, slowed turnover of mitochondria does not result in increased mitochondrial mass in p.D146N cells, suggesting a putative 'negative feedback' on mitochondrial biogenesis [AFG3-like matrix AAA peptidase subunit 2 (AFG3L2) levels in WB in Fig. 2A and Fig. 6B]. We also detected accumulation of oxidized mitochondrial proteins in p.D146N fibroblasts, which is likely a consequence of inefficient mitophagy rather than defective oxidative phosphorylation, as measurement of ATP in freshly isolated mitochondria revealed comparable levels in the patient and controls.

We demonstrated that p.D146N mutation has great impact on peroxisomal network and shape. It is noteworthy that this phenotype is not present in fibroblasts from the p.G32A DRP1 patient (20), highlighting the key role of D146 residue for DRP1 functionality and the different behavior of DRP1 mutations, even in the same domain. The interconnected structure of peroxisomes we found in p.D146N cells is in accordance with the shared function of DRP1 in mediating peroxisomal and mitochondrial fission processes (4). However, the elongation of peroxisomes has been seen only in some DRP1 mutations, independently from their localization in the middle or in the GTPase domain (6,12,16,17). The reason why DRP1 mutations always impact on mitochondrial morphology while only rarely affect peroxisomal division still remains unknown. Interestingly, our results may help in clarifying this discrepancy, by highlighting differential regulatory mechanisms that peroxisomes possess compared to mitochondria. We found increased number of cells presenting elongated peroxisomes and increased peroxisomal mass in p.D146N cells. More intriguingly, we noticed a much greater raise in peroxisomal catalase, exceeding the mass increase. These data could be explained as a peroxisomal response to its own defect, but also as a reaction to mitochondrial oxidative stress. Indeed, the physiological interplay between these two organelles has been already widely recognized, which communicate to each other through exchanging ROS, lipids and metabolites; mitochondria-derived vesicles trafficking and establishing physical contact sites, besides sharing division machinery components and responses in antiviral signaling (4). What is still not clarified is their mutual crosstalk in pathological conditions, affecting one organelle or the other. In this context, it is noteworthy to mention that also primary defects in peroxisomal function lead to neurological phenotypes (5). The fact that not all DRP1 mutations that lead to a peroxisomal morphology alteration may be ascribable to a 'peroxisomal resistance' to some dysfunctions, since they have been shown to largely antagonize oxidative stress when it originates within mitochondria (33). Indeed, and in support to our increased catalase expression data, it has been demonstrated that peroxisomes exert a compensatory function toward mitochondria, as enhanced peroxisomal catalase function restores mitochondrial depolarization and ROS accumulation (5), and peroxisome proliferation ameliorates mitochondrial dysfunction in neurodegenerative neuronal models (34).

This work, as first, uncovers the relative role of disrupted homeostasis of mitochondria and peroxisomes. Consequently, we can consider mutations in DRP1 as 'true mitostatic disorders,' being DRP1 directly linked to mitochondrial turnover, especially to mitochondrial dynamics and mitophagy.

Materials and methods

Samples for genetic analysis

This investigation conformed to principles outlined in the Declaration of Helsinki. Clinical and family history details were collected during genetic counseling, and written informed consents were obtained from both parents. Genetic analysis was performed in the symptomatic index case and unaffected parents. Genomic DNA (gDNA) was extracted from peripheral blood using the automated extractor Maxwell16 (Promega, Milano, Italy); the concentration and gDNA quality were determined using Qubit® Fluorometer (ThermoFisher Scientific).

Library enrichment and next generation sequencing

Sample enrichment and paired-end libraries preparation were performed using the commercial kit TruSight One (Illumina, San Diego, CA, USA), following the manufacturer's instructions (Document #1000000006694 v00). TruSight One Sequencing panel includes 4813 genes associated with known clinical phenotypes (clinical exome), selected according to the Human Gene Mutation Database (HGMD, http://www.hgmd.cf.ac.uk/ac/index.php), OMIM (www.omim.org) and GeneTests (www.genetests.org). The entire gene list is published on Illumina website (www.illumina.com/content/dam/illumina-marketing/documents/products/technotes/technote_trusight_one_panel.pdf).

For enrichment 50 ng of gDNA for each sample was used, and the concentration and size distribution of the obtained libraries were determined on Agilent Bioanalyzer DNA 1000 chip (Agilent Technologies, USA). Final libraries were pooled, and sequencing was performed on MiSeq instrument (Illumina, San Diego, CA, USA) with a flow cell V3, 600 cycles PE.

Next generation sequencing data analysis

Paired-end reads were mapped against the National Center for Biotechnology Information (NCBI) human reference genome build GRCh37. Read alignment and variant calling were performed with MiSeq Reporter software, and all variants were then annotated using Illumina VariantStudio data analysis software.

For the identification of possible causative variants, restrictive filters were applied: (1) minor allele frequency <1% in 1000 Genomes and ExAC database; (2) the localization of detected variants, considering only exonic and intronic variations at ± 20 bp from the coding regions; (3) *de novo* or autosomal recessive inheritance model.

Interpretation of putative variants was performed using Alamut® Visual (Interactive Biosoftware), integrating data from several databases, such as NCBI, UCSC, Clinical Variation and HGMD, and *in silico* prediction tools such as Polyphen (35), Sift (36), UMD predictor (37) and phyloP for conservation score. Candidate variants were classified according to ACMG criteria in 5 categories [class 1: benign, class 2: likely benign, class 3: variant of uncertain significance (VUS), class 4: likely pathogenic, class 5: pathogenic] (38).

Candidate variants were confirmed by Sanger sequencing. on AB3730 DNA sequencer (Applied Biosystem).

Muscle biopsy, fibroblast cell culture and EM

Muscle biopsy was performed in the quadriceps as previously described (39).

Fibroblasts were generated and cultured from skin biopsy for the patient. Age-matched controls were from ATCC cell line. Cells were grown in Dulbecco's modified Eagle's medium supplemented with 20% fetal bovine serum, 1 mM sodium pyruvate, 2 mM L-glutamine and 100 U/mL penicillin–streptomycin (all components from GIBCO). Electron microscopy (EM) was performed as described (40).

SDS-PAGE, Native-PAGE, WB analysis

Primary fibroblasts were lysed in 100 mM Tris–HCl pH 7.4, 150 mM NaCl, 1 mM EDTA pH 8.0, 1% Triton X-100 for sodium dodecyl sulfate (SDS) or 0.1% for Native-PAGE, protease inhibitor cocktail (Sigma-Aldrich) 1:1000, incubated on ice for 30 minutes and centrifuged to remove nuclei and cell debris. Protein quantification was performed by Bradford assay according to the manufacturer's instructions. Samples were loaded in a Native-PAGE (standard polyacrylamide gel without SDS detergent and sample resuspension in non-reducing non-denaturing sample buffer) or SDS-PAGE and then subjected to WB analysis. Western blot primary antibodies: anti-DRP1 (ab184247, Abcam); anti–glyceraldehyde-3-phosphate dehydrogenase (GAPDH) (sc-32233, Santa Cruz); anti-AFG3L2 (homemade); anti–mitochondrial import inner membrane translocase subunit 44 (TIM44) (ab194829, Abcam); anti-HA (clone 16812, Biolegend); anti–β-actin [13E5, horseradish peroxidase (HRP) conjugate, #5125, Cell Signaling]; anti-LC3 A/B (ab58610, Abcam); anti-catalase (ab16731, Abcam); anti-PMP70 (ab3421, Abcam) and anti–actin-related protein 2/3 complex subunit 2 (ARPC2) (clone5C8, WH0010109M1, Sigma-Aldrich). Secondary antibodies: electrochemiluminescence anti-mouse and anti-rabbit immunoglobulin G, HRP-linked species-specific whole antibodies from Amersham Bioscience (NA931 and NA934).

Mitochondrial morphology network study

For mitochondrial morphology analysis, 20 000 cells were plated on a bottom-glass culture dish (Matteck) and 24 hours later infected with lentivirus expressing mito-DsRed2 (41). Seventy-two hours after the infection, mitochondrial network morphology was evaluated in live imaging using an Axio Observer.Z1 inverted microscope (Zeiss), at 40× objective.

Primary fibroblast transfection

Twenty thousand patient and control fibroblasts were plated on a bottom-glass culture dish (Matteck) and 24 hours later transfected by using Lipofectamine 2000 (Invitrogen) following the manufacturer's instructions. Constructs employed were pEYFP-Mito Vector (#6115-1, Clontech) + pcDNA3 expressing wild-type or mutagenized DRP1 (see Site-Directed Mutagenesis), kindly given by L. Scorrano (22), or pEYFP-Mito Vector plus empty backbone control (pcDNA 3.1, Invitrogen). pcDNA3-DRP1 (mutant or wild type) was transfected in a ratio of 2:1 respect to the pEYFP-Mito Vector. Forty-eight or 24 hours after transfection, cells were acquired in live imaging using an Axio Observer.Z1 inverted microscope (Zeiss).

Site-directed mutagenesis

We generated mutant DRP1 constructs using QuikChange Lightning Kit (#210519, Agilent Technologies). We introduced the following mutations: p.D146N, p.G32A (20) and p. L406S (17) mutations. Obtained plasmids were Sanger sequenced by Eurofins Genomics to confirm mutagenesis of the specific residues.

Mitochondria purification

Ten million patient and control fibroblasts were collected and washed in phosphate-buffered saline (PBS). Mitochondria Isolation Kit (Miltenyi Biotec) was used to purify Mito from the cytosol following the manufacturer's instruction (42).

Mitochondrial turnover assay

Cells were transfected as described with pTRE-Tight-MitoTimer construct (Plasmid number 50547, Addgene) plus plasmid expressing rtTA (Tet-ON). Twenty-four hours after transfection, the expression of the transgene was induced with 4 µg/mL of doxycycline for 1 hour and then removed from the media to analyze it at different times (4, 28 and 52 hours from induction). Quantification was calculated as the mean loss of red fluorescence intensity at each time point comparing control and patient cells and then plotted as a percentage.

Autophagic flux analysis

Fibroblasts were plated in six-multiwell plates and after 24 hours treated for 6 hours with chloroquine 50 µM (Sigma-Aldrich) to block lysosomal degradation or vehicle (water). Vehicle-treated or drug-treated cells were harvested and subjected to WB analysis.

Immunofluorescence analyses

Cells were plated on glass coverslips and fixed with 4% paraformaldehyde. Then cells were permeabilized and blocked by incubation in PBS, 10% normal goat serum and 0.5% Triton X-100 and incubated with primary antibody buffered in PBS, 5% normal goat serum, and 0.1% Triton X-100 overnight at 4°C. Cells were then incubated with secondary antibody and counterstained with DAPI. Primary antibodies: Alexa-Fluor 568 Phalloidin (A12380, ThermoFisher Scientific) and anti-PMP70 (CL2524, NBP2-36770, Novusbio). Secondary antibodies were Alexa-Fluor 488 goat anti-mouse from Invitrogen (A32731).

Detection of mitochondrial carbonylated proteins

Total homogenates and mitochondrial fractions were subjected to OxyBlot Protein Oxidation Detection Kit (Millipore, #S7150), which employs the derivatization of the carbonyl groups of oxidized proteins to 2,4-dinitrophenylhydrazone (DNP-hydrazone) by reaction with 2,4-dinitrophenylhydrazine (DNPH). The DNP-derivatized (DNP+) and non-derivatized (DNP−) protein samples are separated by PAGE followed by WB and detected by specific anti-DNP+ antibody provided in OxyBlot Protein Oxidation Detection Kit.

Mitochondrial ATP production

We measured ATP production in freshly isolated mitochondria from fibroblasts, as described (43). Mitochondria were isolated by differential centrifugation and incubated at 37°C for 30 minutes in a respiratory buffer (0.25 M sucrose, 20 mM MOPS, 1 mM EDTA, 5 mM inorganic phosphate, 0.1% BSA fatty acid free and 1 mM ADP, pH 7.4). By providing pyruvate/malate (5 and 1 mM,

respectively) or glutamate/malate (5 and 1 mM, respectively) as substrates, we stimulated ATP synthesis dependent on complexes I, II, III, IV and V. ATP production was measured by luminometric assay as described (43).

Confocal microscopy and analysis of cells presenting elongated peroxisomes

Immunofluorescence experiments were acquired both at Axio Imager Upright Microscope (Zeiss) with 63× oil objective and at confocal microscope Perkin Elmer UltraVIEW ERS with 63× oil objective and sectioned in Z stacks of 0.1 µm. Volocity software was used to acquire images. Analysis of cells was performed counting the number of cells presenting dot-like or elongated peroxisomes and expressed as a percentage (at least 50 cells per genotype).

Statistical analyses

Mean values of the two controls are compared with mean values of the patient in independent experiments, by two-sample equal variance (homoscedastic) and two-tailed *t* test and reported in graphs as mean ± standard error of the mean (SEM); $^{*}P < 0.05$, $^{**}P < 0.01$, $^{***}P < 0.001$.

Acknowledgements

We would like to acknowledge Dr. Vidmer Scaioli for his valuable contribution through the fine interpretation of electroneuronography, Isabella Lorenzetti for technical assistance in muscle biopsy staining, Paola Podini for technical processing of EM and the family for their permission to publish this article. We thank Simone Cenci and Enrico Milan for the suggestions in the interpretation of autophagic flux study; ALEMBIC (advanced microscopy laboratory Facility) of IRCCS Ospedale San Raffaele and Cesare Covino for suggestions in immunofluorescence analyses. S.C.P. was supported by the Italian Ministry of Health (RF-2011-02347127) and CoFin Regione Lombardia (n. 96.), FM by the Italian Ministry of Health (RF-2016-02361610).

Conflict of Interest statement. None declared.

References

1. Tilokani, L., Nagashima, S., Paupe, V. and Prudent, J. (2018) Mitochondrial dynamics: overview of molecular mechanisms. *Essays Biochem.*, **62**, 341–360.
2. Misgeld, T. and Schwarz, T.L. (2017) Mitostasis in neurons: maintaining mitochondria in an extended cellular architecture. *Neuron*, **96**, 651–666.
3. Twig, G., Elorza, A., Molina, A.J., Mohamed, H., Wikstrom, J.D., Walzer, G., Stiles, L., Haigh, S.E., Katz, S., Las, G. *et al.* (2008) Fission and selective fusion govern mitochondrial segregation and elimination by autophagy. *EMBO J.*, **27**, 433–446.
4. Schrader, M., Bonekamp, N.A. and Islinger, M. (2012) Fission and proliferation of peroxisomes. *Biochim. Biophys. Acta*, **1822**, 1343–1357.
5. Fransen, M., Lismont, C. and Walton, P. (2017) The peroxisome-mitochondria connection: how and why? *Int. J. Mol. Sci.*, **18**.
6. Waterham, H.R., Koster, J., van Roermund, C.W., Mooyer, P.A., Wanders, R.J. and Leonard, J.V. (2007) A lethal defect of mitochondrial and peroxisomal fission. *N. Engl. J. Med.*, **356**, 1736–1741.
7. Chang, C.R., Manlandro, C.M., Arnoult, D., Stadler, J., Posey, A.E., Hill, R.B. and Blackstone, C. (2010) A lethal de novo mutation in the middle domain of the dynamin-related GTPase Drp1 impairs higher order assembly and mitochondrial division. *J. Biol. Chem.*, **285**, 32494–32503.
8. Chao, Y.H., Robak, L.A., Xia, F., Koenig, M.K., Adesina, A., Bacino, C.A., Scaglia, F., Bellen, H.J. and Wangler, M.F. (2016) Missense variants in the middle domain of DNM1L in cases of infantile encephalopathy alter peroxisomes and mitochondria when assayed in *Drosophila*. *Hum. Mol. Genet.*, **25**, 1846–1856.
9. Vanstone, J.R., Smith, A.M., McBride, S., Naas, T., Holcik, M., Antoun, G., Harper, M.E., Michaud, J., Sell, E., Chakraborty, P. *et al.* (2016) DNM1L-related mitochondrial fission defect presenting as refractory epilepsy. *Eur. J. Hum. Genet.*, **24**, 1084–1088.
10. Fahrner, J.A., Liu, R., Perry, M.S., Klein, J. and Chan, D.C. (2016) A novel de novo dominant negative mutation in DNM1L impairs mitochondrial fission and presents as childhood epileptic encephalopathy. *Am. J. Med. Genet. A*, **170**, 2002–2011.
11. Sheffer, R., Douiev, L., Edvardson, S., Shaag, A., Tamimi, K., Soiferman, D., Meiner, V. and Saada, A. (2016) Postnatal microcephaly and pain insensitivity due to a de novo heterozygous DNM1L mutation causing impaired mitochondrial fission and function. *Am. J. Med. Genet. A*, **170**, 1603–1607.
12. Diez, H., Cortes-Saladelafont, E., Ormazabal, A., Marmiese, A.F., Armstrong, J., Matalonga, L., Bravo, M., Briones, P., Emperador, S., Montoya, J. *et al.* (2017) Severe infantile parkinsonism because of a de novo mutation on DLP1 mitochondrial-peroxisomal protein. *Mov. Disord.*, **32**, 1108–1110.
13. Ryan, C.S., Fine, A.L., Cohen, A.L., Schiltz, B.M., Renaud, D.L., Wirrell, E.C., Patterson, M.C., Boczek, N.J., Liu, R., Babovic-Vuksanovic, D. *et al.* (2018) De novo DNM1L variant in a teenager with progressive paroxysmal dystonia and lethal super-refractory myoclonic status Epilepticus. *J. Child Neurol.*, **33**, 651–658.
14. Ladds, E., Whitney, A., Dombi, E., Hofer, M., Anand, G., Harrison, V., Fratter, C., Carver, J., Barbosa, I.A., Simpson, M. *et al.* (2018) De novo DNM1L mutation associated with mitochondrial epilepsy syndrome with fever sensitivity. *Neurol. Genet.*, **4**, e258.
15. Yoon, G., Malam, Z., Paton, T., Marshall, C.R., Hyatt, E., Ivakine, Z., Scherer, S.W., Lee, K.S., Hawkins, C., Cohn, R.D. *et al.* (2016) Lethal disorder of mitochondrial fission caused by mutations in DNM1L. *J. Pediatr.*, **171**, 313–316.
16. Nasca, A., Legati, A., Baruffini, E., Nolli, C., Moroni, I., Ardissone, A., Goffrini, P. and Ghezzi, D. (2016) Biallelic mutations in DNM1L are associated with a slowly progressive infantile encephalopathy. *Hum. Mutat.*, **37**, 898–903.
17. Zaha, K., Matsumoto, H., Itoh, M., Saitsu, H., Kato, K., Kato, M., Ogata, S., Murayama, K., Kishita, Y., Mizuno, Y. *et al.* (2016) DNM1L-related encephalopathy in infancy with Leigh syndrome-like phenotype and suppression-burst. *Clin. Genet.*, **90**, 472–474.
18. Hogarth, K.A., Costford, S.R., Yoon, G., Sondheimer, N. and Maynes, J.T. (2018) DNM1L variant alters baseline mitochondrial function and response to stress in a patient with severe neurological dysfunction. *Biochem. Genet.*, **56**, 56–77.
19. Gerber, S., Charif, M., Chevrollier, A., Chaumette, T., Angebault, C., Kane, M.S., Paris, A., Alban, J., Quiles, M., Delettre, C. *et al.* (2017) Mutations in DNM1L, as in OPA1, result in

dominant optic atrophy despite opposite effects on mitochondrial fusion and fission. *Brain*, **140**, 2586–2596.
20. Whitley, B.N., Lam, C., Cui, H., Haude, K., Bai, R., Escobar, L., Hamilton, A., Brady, L., Tarnopolsky, M.A., Dengle, L. *et al.* (2018) Aberrant Drp1-mediated mitochondrial division presents in humans with variable outcomes. *Hum. Mol. Genet.*, **27**, 3710–3719.
21. Wenger, J., Klinglmayr, E., Frohlich, C., Eibl, C., Gimeno, A., Hessenberger, M., Puehringer, S., Daumke, O. and Goettig, P. (2013) Functional mapping of human dynamin-1-like GTPase domain based on x-ray structure analyses. *PLoS One*, **8**, e71835.
22. Smirnova, E., Griparic, L., Shurland, D.L. and van der, A.M. (2001) Dynamin-related protein Drp1 is required for mitochondrial division in mammalian cells. *Mol. Biol. Cell*, **12**, 2245–2256.
23. Hernandez, G., Thornton, C., Stotland, A., Lui, D., Sin, J., Ramil, J., Magee, N., Andres, A., Quarato, G., Carreira, R.S. *et al.* (2013) MitoTimer: a novel tool for monitoring mitochondrial turnover. *Autophagy*, **9**, 1852–1861.
24. Klionsky, D.J., Abdelmohsen, K., Abe, A., Abedin, M.J., Abeliovich, H., Acevedo Arozena, A., Adachi, H., Adams, C.M., Adams, P.D., Adeli, K. *et al.* (2016) Guidelines for the use and interpretation of assays for monitoring autophagy (3rd edition). *Autophagy*, **12**, 1–222.
25. Ferrari, L.F., Chum, A., Bogen, O., Reichling, D.B. and Levine, J.D. (2011) Role of Drp1, a key mitochondrial fission protein, in neuropathic pain. *J. Neurosci.*, **31**, 11404–11410.
26. Pareyson, D., Piscosquito, G., Moroni, I., Salsano, E. and Zeviani, M. (2013) Peripheral neuropathy in mitochondrial disorders. *Lancet Neurol.*, **12**, 1011–1024.
27. Huber, N., Guimaraes, S., Schrader, M., Suter, U. and Niemann, A. (2013) Charcot-Marie-tooth disease-associated mutants of GDAP1 dissociate its roles in peroxisomal and mitochondrial fission. *EMBO Rep.*, **14**, 545–552.
28. Wong, Y.C., Ysselstein, D. and Krainc, D. (2018) Mitochondria-lysosome contacts regulate mitochondrial fission via RAB7 GTP hydrolysis. *Nature*, **554**, 382–386.
29. Houlden, H., King, R.H., Muddle, J.R., Warner, T.T., Reilly, M.M., Orrell, R.W. and Ginsberg, L. (2004) A novel RAB7 mutation associated with ulcero-mutilating neuropathy. *Ann. Neurol.*, **56**, 586–590.
30. Ban-Ishihara, R., Ishihara, T., Sasaki, N., Mihara, K. and Ishihara, N. (2013) Dynamics of nucleoid structure regulated by mitochondrial fission contributes to cristae reformation and release of cytochrome c. *Proc. Natl. Acad. Sci. USA*, **110**, 11863–11868.
31. Lewis, S.C., Uchiyama, L.F. and Nunnari, J. (2016) ER-mitochondria contacts couple mtDNA synthesis with mitochondrial division in human cells. *Science*, **353**, aaf5549.
32. Wakabayashi, J., Zhang, Z., Wakabayashi, N., Tamura, Y., Fukaya, M., Kensler, T.W., Iijima, M. and Sesaki, H. (2009) The dynamin-related GTPase Drp1 is required for embryonic and brain development in mice. *J. Cell Biol.*, **186**, 805–816.
33. Ivashchenko, O., Van Veldhoven, P.P., Brees, C., Ho, Y.S., Terlecky, S.R. and Fransen, M. (2011) Intraperoxisomal redox balance in mammalian cells: oxidative stress and interorganellar cross-talk. *Mol. Biol. Cell*, **22**, 1440–1451.
34. Santos, M.J., Quintanilla, R.A., Toro, A., Grandy, R., Dinamarca, M.C., Godoy, J.A. and Inestrosa, N.C. (2005) Peroxisomal proliferation protects from beta-amyloid neurodegeneration. *J. Biol. Chem.*, **280**, 41057–41068.
35. Adzhubei, I.A., Schmidt, S., Peshkin, L., Ramensky, V.E., Gerasimova, A., Bork, P., Kondrashov, A.S. and Sunyaev, S.R. (2010) A method and server for predicting damaging missense mutations. *Nat. Methods*, **7**, 248–249.
36. Choi, Y., Sims, G.E., Murphy, S., Miller, J.R. and Chan, A.P. (2012) Predicting the functional effect of amino acid substitutions and indels. *PLoS One*, **7**, e46688.
37. Salgado, D., Desvignes, J.P., Rai, G., Blanchard, A., Miltgen, M., Pinard, A., Levy, N., Collod-Beroud, G. and Beroud, C. (2016) UMD-predictor: a high-throughput sequencing compliant system for pathogenicity prediction of any human cDNA substitution. *Hum. Mutat.*, **37**, 439–446.
38. Richards, S., Aziz, N., Bale, S., Bick, D., Das, S., Gastier-Foster, J., Grody, W.W., Hegde, M., Lyon, E., Spector, E. *et al.* (2015) Standards and guidelines for the interpretation of sequence variants: a joint consensus recommendation of the American College of Medical Genetics and Genomics and the Association for Molecular Pathology. *Genet. Med.*, **17**, 405–424.
39. Benedetti, S., Bertini, E., Iannaccone, S., Angelini, C., Trisciani, M., Toniolo, D., Sferrazza, B., Carrera, P., Comi, G., Ferrari, M. *et al.* (2005) Dominant LMNA mutations can cause combined muscular dystrophy and peripheral neuropathy. *J. Neurol. Neurosurg. Psychiatry*, **76**, 1019–1021.
40. Quattrini, A., Previtali, S., Feltri, M.L., Canal, N., Nemni, R. and Wrabetz, L. (1996) b4 integrin and other Schwann cell markers in axonal neuropathy. *Glia*, **17**, 294–306.
41. Hirai, H. (2008) Progress in transduction of cerebellar Purkinje cells in vivo using viral vectors. *Cerebellum*, **7**, 273–278.
42. Franko, A., Baris, O.R., Bergschneider, E., von Toerne, C., Hauck, S.M., Aichler, M., Walch, A.K., Wurst, W., Wiesner, R.J., Johnston, I.C. *et al.* (2013) Efficient isolation of pure and functional mitochondria from mouse tissues using automated tissue disruption and enrichment with anti-TOM22 magnetic beads. *PLoS One*, **8**, e82392.
43. Maltecca, F., Aghaie, A., Schroeder, D.G., Cassina, L., Taylor, B.A., Phillips, S.J., Malaguti, M., Previtali, S., Guenet, J.L., Quattrini, A. *et al.* (2008) The mitochondrial protease AFG3L2 is essential for axonal development. *J. Neurosci.*, **28**, 2827–2836.
44. Verrigni, D., Di Nottia, M., Ardissone, A., Baruffini, E., Nasca, A., Legati, A., Bellacchio, E., Fagiolari, G., Martinelli, D., Fusco, L. *et al.* (2019) Clinical-genetic features and peculiar muscle histopathology in infantile DNM1L-related mitochondrial epileptic encephalopathy. *Hum. Mutat.*, **40**, 601–618.
45. Assia Batzir, N., Bhagwat, P., Eble, T., Liu, P., Eng, C., Elsea, S.H., Robak, L.A., Scaglia, F., Goldman, A., Dhar, S.U. *et al.* (2019) De novo missense variant in the GTPase effector domain (GED) of DNM1L leads to static encephalopathy and seizures. *Cold Spring Harb. Mol. Case Stud.*, **5**.